Letter Vol. 44, No. 24 / 15 December 2019 / Optics Letters 6041

Anomalous plasmon hybridization in nanoantennas near interfaces

JINGXUAN WEI[1,2] AND CHENGKUO LEE[1,2,*]

[1]Department of Electrical and Computer Engineering, National University of Singapore, Singapore 117583, Singapore
[2]Center for Intelligent Sensors and MEMS, National University of Singapore, Singapore 117581, Singapore
*Corresponding author: elelc@nus.edu.sg

Received 22 October 2019; revised 16 November 2019; accepted 18 November 2019; posted 18 November 2019 (Doc. ID 381183); published 10 December 2019

We report on an anomalous plasmon hybridization in side-by-side coupled metallic nanoantennas on top of a silicon waveguide. Contrary to the conventional perception based on Coulomb coupling, the hybridized anti-symmetric mode in our structure possesses a higher resonance frequency than the symmetric mode. This unusual phenomenon reveals a new mechanism of plasmon hybridization, namely, coupling-induced charge redistribution. Our work includes numerical simulation, experimental validation, and theoretical analysis, emphasizing the importance of dielectric interfaces in coupled plasmonic structures, and offers new possibilities for non-Hermitian systems and integrated devices.

https://doi.org/10.1364/OL.44.006041

Localized surface plasmon resonance (LSPR) is the collective oscillation of electrons in isolated metallic structures [1]. When two plasmonic structures are close to each other, new resonant modes are formed with a splitting in the resonance frequency, which is referred to as plasmon hybridization [2]. Plasmon hybridization enables a plethora of intriguing phenomena, including Fano resonance [3,4], bright and dark modes [5,6], electromagnetically induced transparency [7,8], and superscattering [9]. These phenomena have found widespread applications in various research areas. For example, Fano resonance features sharp asymmetric far-field spectra, which are widely used in sensors [10,11] and modulators [12,13]. To fully exploit the benefits of hybridized modes, a comprehensive understanding of the mechanism of plasmon hybridization is required, which has attracted continuous attention over the past decade [14–19].

A widely used theoretical framework of plasmon hybridization is based on the Coulomb coupling at electrostatic approximation [19]. To calculate the coupling strength, the surface charge distribution of individual plasmons should be simulated or calculated as the first step. Then, a double integral should be performed over the surfaces of two particles to obtain the total electrostatic interaction. In the calculation, the surface charge distribution of plasmonic particles is assumed not to be affected by the interaction [19,20]. This conventional method has achieved great success in explaining many phenomena. However, this model does not include the effect of mutual coupling on the eigenmodes, or surface charge distribution of individual plasmons. Although a similar effect plays an important role in the formation of molecular bonds [21], a counterpart of plasmon hybridization in quantum chemistry, coupling-induced charge redistribution (CICR), is usually considered as a higher-order perturbation term in plasmons [20]. This occurs because the resonance frequency of plasmons is dependent on the effective refractive index of the environment, which is robust to the surface charge distribution when the medium is homogeneous [22]. In an inhomogeneous environment, however, the effective refractive index may be significantly changed by CICR. So far, the effect of dielectric interfaces on plasmon coupling has not been exploited. This question is not only a fundamental problem of plasmonics but is also interesting for practical designs of the emerging nanoantennas coupled with dielectric waveguides [23–28].

Here, we investigate the plasmon hybridization near dielectric interfaces, revealing an anomalous phenomenon that cannot be explained by the conventional understanding based on Coulomb coupling. This anomalous plasmon hybridization is numerically found in side-by-side coupled metallic nanoantennas on top of a silicon waveguide, in which the hybridized anti-symmetric dark mode possesses a higher resonance frequency than the symmetric bright mode. By examining the field distribution of nanoantennas, we propose a new mechanism of plasmon hybridization, namely, CICR. The effect of the coupling gap on hybridization is also investigated, revealing two different regions where Coulomb coupling and CICR dominate. Experiments using double L-shaped nanoantennas in an out-of-plane configuration support our analysis. The effect of CICR can be included in a theoretical framework using coupled mode theory. Our findings will not only be interesting for on-chip devices, but also open new possibilities for non-Hermitian systems where tunable coupling is highly desired.

Figure 1(a) shows the schematic of side-by-side coupled cut-wire nanoantennas on a silicon waveguide with a thin silicon dioxide spacer. The inset shows the cross section of the side view. The length (L_{ant}), width (W_{ant}), and thickness (T_{ant}) of the nanoantennas are 1.1 μm, 0.1 μm, and 0.1 μm, respectively. The gap between two nanoantennas is 0.1 μm. The width (W_{wg})

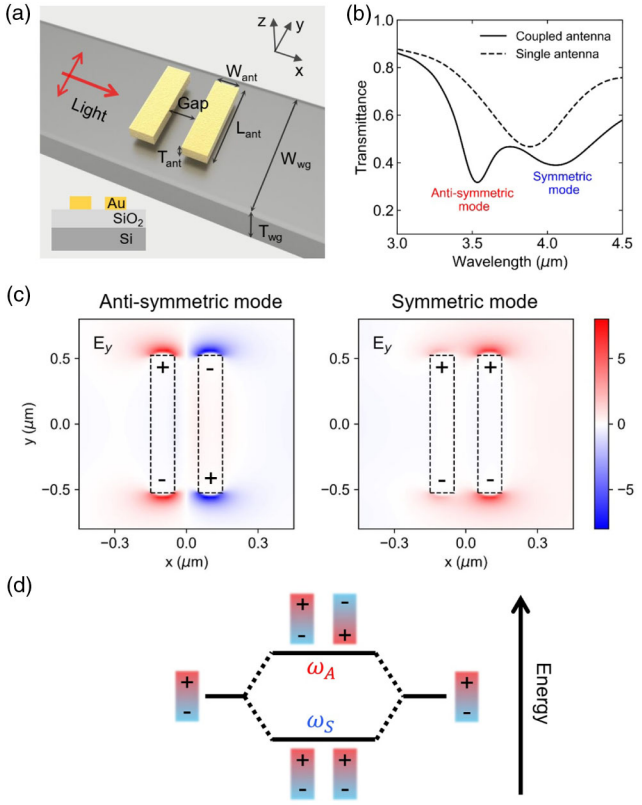

Fig. 1. Observation of anomalous plasmon hybridization in coupled nanoantennas near interfaces. (a) Schematic of cut-wire nanoantennas on top of silicon waveguide. L_{ant}, W_{ant}, and T_{ant} are 1.1 μm, 0.1 μm, and 0.1 μm, respectively. Gap is 0.1 μm. Inset: side view of the structure. (b) Simulated transmittance spectra for single cut-wire (solid line) and coupled cut-wire (broken line) nanoantennas. (c) Real part of electric field (E_y) of the hybridized anti-symmetric and symmetric modes. (d) Schematic energy diagram of the anomalous plasmon hybridization.

and thickness (T_{wg}) of the silicon waveguide are 1.2 μm and 0.4 μm, respectively. The thickness of the SiO_2 spacer is 0.1 μm. The refractive indices of gold, silicon, and silicon dioxide are taken from Palik's handbook [29]. The mesh size used in the simulations is 5 nm. Figure 1(b) shows the simulated transmittance spectra using the finite-difference time-domain (FDTD) method. The input light is transverse electric mode with polarization along y direction. The narrow and broad transmission dips around 3.5 μm and 4.1 μm wavelength represent the hybridized anti-symmetric and symmetric plasmonic modes, respectively. The bandwidth of the anti-symmetric mode is narrower because it is relatively darker than the symmetric mode. We also simulate the transmittance spectra of a single cut-wire nanoantenna, which shows only one dip around 3.8 μm. The resonance wavelength of the single nanoantenna lies between those of coupled nanoantennas, which is a typical phenomenon of plasmon hybridization [18].

Based on the conventional conception on plasmon hybridization, the side-by-side coupling in such a parallel placed nanoantenna pair should lead to a bright symmetric mode and a dark anti-symmetric mode, which possess higher and lower resonance frequencies, respectively [19,30]. In other words, the resonance wavelength of the dark anti-symmetric mode should be longer than that of the single nanoantenna and bright symmetric mode. However, the plasmon hybridization in our structure is reversed, namely, the dark anti-symmetric mode possesses a shorter resonance wavelength than the bright symmetric mode. This unusual phenomenon is verified by the simulated electric field (Re(E_y)) distribution, as shown in Fig. 1(c). The asymmetric field distribution for the bright mode is due to the interplay between the anti-symmetric and symmetric modes, leading to constructive interference on one nanoantenna and destructive interference on the other. This effect is typical in non-Hermitian systems, where resonators are coupled by decaying into the same channel, e.g., radiation to the far field [31,32]. An energy diagram describing the anomalous plasmon hybridization is illustrated in Fig. 1(d), where the energy of plasmon is proportional to the inverse of resonance wavelength.

Intuitively, this unusual behavior of plasmon hybridization should result from the asymmetry introduced by the dielectric interfaces, where the field distribution of the nanoantennas is affected significantly due to the mutual coupling. To confirm our hypothesis, we examine the amplitude of the electric field, |**E**|, along the cross section, as shown in Fig. 2. Around 3.5 μm wavelength, the electric field of the anti-symmetric mode is distributed mainly in air, of which the refractive index (n) is 1. In contrast, for the symmetric mode around 4.1 μm, the majority of the electric field is buried in the SiO_2 substrate ($n = 1.4$). The asymmetric electric field distribution near the interfaces can be understood by Maxwell equations [33]. Furthermore, as we can see in the XZ plane, the electric field in air is localized mainly in the gap for 3.5 μm resonance. According to Gauss's law, this field distribution indicates that the surface charges are accumulated on the side walls of nanoantennas due to the electrostatic attraction. On the other hand, for the symmetric mode at 4.1 μm, the surface charges are repelled to the dielectric–metal interfaces, and the field is distributed mainly in dielectrics. In summary, more surface charges are attracted from the dielectric surfaces to the side walls of nanoantennas in the anti-symmetric mode, leading to a decrease in effective refractive index and hence a decrease in resonance frequency. It is worth noting that this anomalous hybridization is unlikely due to the magnetic interaction of induced currents in nanoantennas, because the electric field dominates in the near field [19]. Considering the very small gap and spacing layer, this effect is unlikely due to propagating waves along the surfaces or multilayer interference. Therefore, we argue that the anomalous plasmon hybridization can be explained by the effect of CICR in nanoantennas near interfaces.

To gain more insight into anomalous plasmon hybridization, we simulate the transmittance spectra for different coupling gaps, as shown in Fig. 3. For increasing gaps, the anti-symmetric mode is first blue-shifted and then red-shifted. A minimum resonance wavelength is achieved when the gap approaches 0.1 μm. The non-monotonous dependence reveals two distinct regions where different mechanisms of plasmon hybridization dominate. When the gap is below 0.1 μm, the blue shift of the anti-symmetric mode can be explained by the conventional understanding based on Coulomb coupling. When the gaps become larger, since the Coulomb coupling decays fast with distance in the near field [30,34], CICR becomes dominant. This suggests CICR is a relatively long-range effect, which still plays a role even when the gap is above 500 nm.

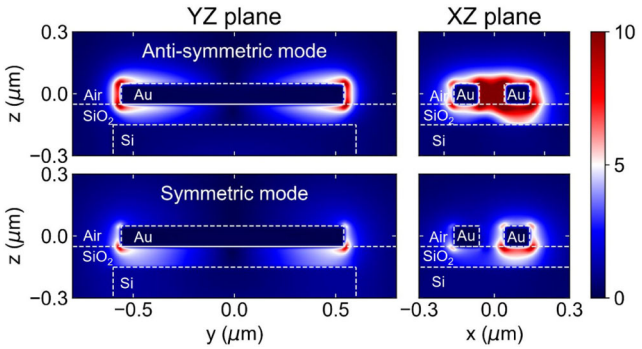

Fig. 2. Simulated electric field (|**E**|) in the YZ (front view) and XZ (side view) planes. While the majority of the |**E**| field is distributed in air ($n = 1$) for the anti-symmetric mode at 3.5 μm, most of the |**E**| field is distributed in dielectric ($n = 1.4$) for the symmetric mode at 4.1 μm. The electric field has been normalized to the incident light.

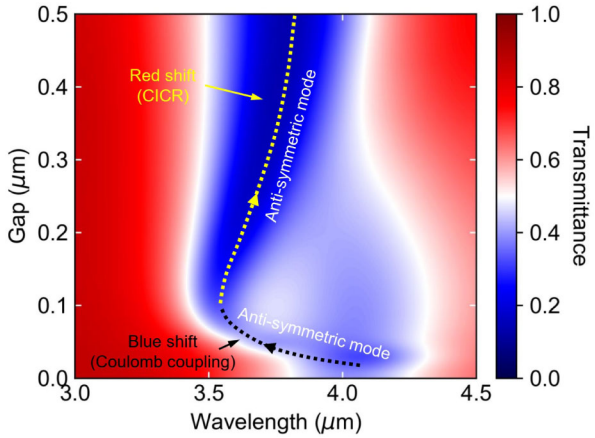

Fig. 3. Simulated transmittance spectra for different coupling gaps. When the gaps increase, the resonance of anti-symmetric mode is first blue-shifted and then red-shifted, indicating that coupling-induced charge redistribution (CICR) is a long-range effect compared to Coulomb coupling.

After the numerical modeling of the anomalous plasmon hybridization due to CICR, we then propose experiments to demonstrate this unusual phenomenon. Considering the relatively low quality factors of metallic nanoantennas, a very broad light source is required to cover both the symmetric and anti-symmetric modes, which is challenging in waveguide-based experiments. Therefore, here we propose experiments in an out-of-plane configuration, using double L-shaped nanoantennas sitting on CaF_2 ($n = 1.4$) substrate, as shown in Fig. 4(a). The advantage of double L-shaped nanoantennas is that pure anti-symmetric and symmetric modes can be excited by controlling the polarization of incident light. In our experiments, nanoantennas with different coupling gaps are fabricated by standard electron beam lithography followed by ebeam evaporation (3/50 nm Ti/Au) and liftoff process. Figure 4(b) shows the scanning electron microscopy images of three typical samples with coupling gaps of 40 nm, 150 nm, and 325 nm. The period of the nanoantennas array along both x and y directions is 2 μm. The scalebars are 1 μm. The measurement is conducted using typical Fourier transform infrared spectroscopy (FTIR). When

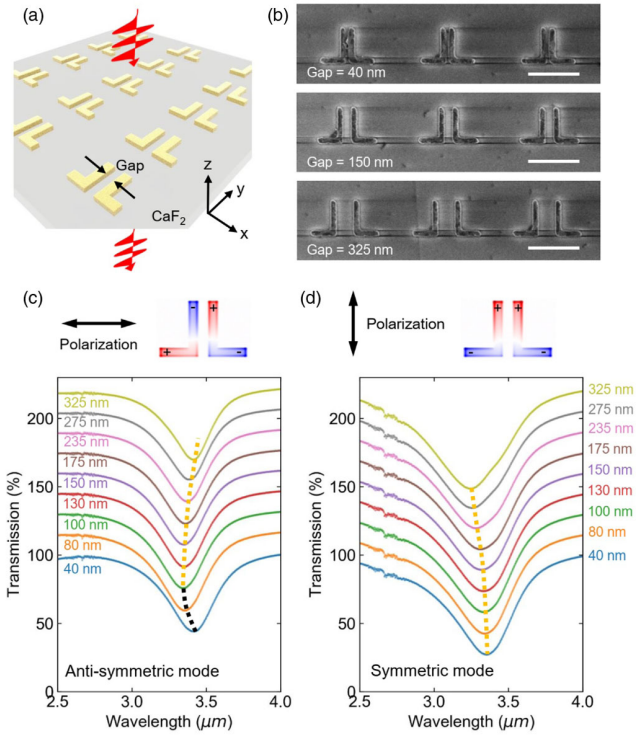

Fig. 4. Experimental validation of the CICR effect using double L-shaped nanoantennas in out-of-plane configuration. (a) Schematic of double L-shaped nanoantennas on CaF_2 substrate for out-of-plane measurement. (b) Scanning electron microscopy images of typical fabricated samples with different coupling gaps (40 nm, 150 nm, 325 nm). The scale bars are 1 μm. Pure (c) anti-symmetric and (d) symmetric modes can be excited in double L-shaped nanoantennas with polarization along x and y directions, respectively. The transmission spectra of the two modes are measured in samples with different gaps, as indicated. Orange curves show the shift of resonance wavelength when CICR is dominated, while the black curve shows the shift of resonance wavelength following Coulomb coupling.

the polarization is along x direction, anti-symmetric modes will be excited, as shown in Fig. 4(c). With increasing gaps, the resonances of the anti-symmetric modes first shift towards a shorter wavelength and then move towards a longer wavelength. This trend reproduces the numerical findings in Fig. 3. On the other hand, when the polarization is along y direction, symmetric modes will be excited, as shown in Fig. 4(d). With increasing gaps, the resonances of symmetric modes move towards a shorter wavelength, which can also be well explained by the effect of CICR.

Mathematically, the effect of CICR can be expressed by the coupled mode theory by adding a new coupling term, γ_{CR}, as follows [32,35]:

$$\frac{d}{dt}\begin{pmatrix} a_1 \\ a_2 \end{pmatrix} = j\begin{pmatrix} \omega_0 & \gamma + \gamma_{CR} \\ \gamma + \gamma_{CR} & \omega_0 \end{pmatrix}\begin{pmatrix} a_1 \\ a_2 \end{pmatrix}, \quad (1)$$

where a_1 and a_2 represent the oscillation amplitude of the two individual nanoantennas. ω_0 is the resonance frequency of a single nanoantenna. $\gamma = \gamma_{NF} + i\gamma_{FF}$ represents the total contribution of near-field and far-field coupling between nanoantennas. As a result, we can calculate the hybridized resonance frequencies of anti-symmetric and symmetric modes,

respectively, as

$$\omega_a = \omega_0 - \gamma_{NF} - i\gamma_{FF} - \gamma_{CR},$$
$$\omega_s = \omega_0 + \gamma_{NF} + i\gamma_{FF} + \gamma_{CR}. \quad (2)$$

Given that the far-field coupling is imaginary [32], the newly formed resonance frequencies of hybridized modes are determined by γ_{NF} and γ_{CR}. When $|\gamma_{NF}| > |\gamma_{CR}|$ or $\gamma_{NF} \cdot \gamma_{CR} > 0$, the overall effect leads to normal plasmon hybridization. However, when $|\gamma_{NF}| < |\gamma_{CR}|$ and $\gamma_{NF} \cdot \gamma_{CR} < 0$, γ_{CR} and γ_{NF} have opposite effects on frequency splitting, and CICR is dominant, leading to an anomalous plasmon hybridization. Therefore, the CICR offers a convenient way to compensate the near-field coupling, which may be interesting for the design of a non-Hermitian system or exceptional point [36,37].

In summary, an anomalous plasmon hybridization has been observed in coupled nanoantennas near interfaces. This unusual phenomenon can be explained by a new mechanism, CICR. While the anomalous plasmon hybridization is studied only numerically, we have experimentally validated the effect of CICR in an out-of-plane configuration. This effect can be theoretically described in the coupled mode theory. Our findings emphasize the effect of interfaces on the plasmon hybridization through changing the distribution of surface charges, opening new possibilities for novel plasmonic designs with applications in non-Hermitian systems and on-chip devices.

Funding. National Research Foundation Singapore (CRP-R263000C24281, ISF-R263000C64281).

Disclosures. The authors declare no conflicts of interest.

REFERENCES

1. S. A. Maier, *Plasmonics: Fundamentals and Applications* (Springer Science & Business Media, 2007).
2. E. Prodan, C. Radloff, N. J. Halas, and P. Nordlander, Science **302**, 419 (2003).
3. B. Luk'Yanchuk, N. I. Zheludev, S. A. Maier, N. J. Halas, P. Nordlander, H. Giessen, and C. T. Chong, Nat. Mater. **9**, 707 (2010).
4. C. Wu, A. B. Khanikaev, R. Adato, N. Arju, A. A. Yanik, H. Altug, and G. Shvets, Nat. Mater. **11**, 69 (2012).
5. F. Hao, Y. Sonnefraud, P. Van Dorpe, S. A. Maier, N. J. Halas, and P. Nordlander, Nano Lett. **8**, 3983 (2008).
6. M. Yorulmaz, A. Hoggard, H. Zhao, F. Wen, W. S. Chang, N. J. Halas, P. Nordlander, and S. Link, Nano Lett. **16**, 6497 (2016).
7. S. Zhang, D. A. Genov, Y. Wang, M. Liu, and X. Zhang, Phys. Rev. Lett. **101**, 047401 (2008).
8. P. Pitchappa, M. Manjappa, C. P. Ho, R. Singh, N. Singh, and C. Lee, Adv. Opt. Mater. **4**, 541 (2016).
9. L. Verslegers, Z. Yu, Z. Ruan, P. B. Catrysse, and S. Fan, Phys. Rev. Lett. **108**, 083902 (2012).
10. G. Dayal, X. Y. Chin, C. Soci, and R. Singh, Adv. Opt. Mater. **5**, 1600559 (2017).
11. Y. Zhang, W. Liu, Z. Li, Z. Li, H. Cheng, S. Chen, and J. Tian, Opt. Lett. **43**, 1842 (2018).
12. T. Lin, F. S. Chau, J. Deng, and G. Zhou, Appl. Phys. Lett. **107**, 223105 (2015).
13. X. Liu, Y. Yu, and X. Zhang, Opt. Lett. **44**, 251 (2019).
14. G. Dolling, C. Enkrich, M. Wegener, J. F. Zhou, C. M. Soukoulis, and S. Linden, Opt. Lett. **30**, 3198 (2005).
15. F. Hao and P. Nordlander, Appl. Phys. Lett. **89**, 103101 (2006).
16. H. Liu, X. Wu, B. Li, C. Xu, G. Zhang, and L. Zheng, Appl. Phys. Lett. **100**, 153114 (2012).
17. Z.-J. Yang, Z.-S. Zhang, Z.-H. Hao, and Q.-Q. Wang, Opt. Lett. **37**, 3675 (2012).
18. N. Liu, H. Guo, L. Fu, S. Kaiser, H. Schweizer, and H. Giessen, Adv. Mater. **19**, 3628 (2007).
19. T. J. Davis and D. E. Gómez, Rev. Mod. Phys. **89**, 011003 (2017).
20. L. Novotny and B. Hecht, *Principles of Nano-Optics* (Cambridge University, 2012).
21. H. Haken and H. C. Wolf, *Molecular Physics and Elements of Quantum Chemistry: Introduction to Experiments and Theory* (Springer Science & Business Media, 2013).
22. L. Novotny, Phys. Rev. Lett. **98**, 266802 (2007).
23. Z. Li, M.-H. Kim, C. Wang, Z. Han, S. Shrestha, A. C. Overvig, M. Lu, A. Stein, A. M. Agarwal, M. Lončar, and N. Yu, Nat. Nanotechnol. **12**, 675 (2017).
24. J. Petersen, J. Volz, and A. Rauschenbeutel, Science **346**, 67 (2014).
25. M. Février, P. Gogol, A. Aassime, R. Mégy, C. Delacour, A. Chelnokov, A. Apuzzo, S. Blaize, J.-M. Lourtioz, and B. Dagens, Nano Lett. **12**, 1032 (2012).
26. R. Guo, M. Decker, F. Setzpfandt, X. Gai, D.-Y. Choi, R. Kiselev, A. Chipouline, I. Staude, T. Pertsch, D. N. Neshev, and Y. S. Kivshar, Sci. Adv. **3**, e1700007 (2017).
27. F. J. Rodríguez-Fortuño, A. Espinosa-Soria, and A. Martínez, J. Opt. **18**, 123001 (2016).
28. F. Peyskens, A. Z. Subramanian, P. Neutens, A. Dhakal, P. Van Dorpe, N. Le Thomas, and R. Baets, Opt. Express **23**, 3088 (2015).
29. E. D. Palik, *Handbook of Optical Constants of Solids*, Vol. **3** (Academic, 1998).
30. A. M. Funston, C. Novo, T. J. Davis, and P. Mulvaney, Nano Lett. **9**, 1651 (2009).
31. S. J. Kim, J.-H. Kang, M. Mutlu, J. Park, W. Park, K. E. Goodson, R. Sinclair, S. Fan, P. G. Kik, and M. L. Brongersma, Nat. Commun. **9**, 316 (2018).
32. S. Yi, M. Zhou, Z. Yu, P. Fan, N. Behdad, D. Lin, K. X. Wang, S. Fan, and M. Brongersma, Nat. Nanotechnol. **13**, 1143 (2018).
33. B. E. A. Saleh and M. C. Teich, *Fundamentals of Photonics* (Wiley, 2019).
34. C. Huck, F. Neubrech, J. Vogt, A. Toma, D. Gerbert, J. Katzmann, T. Härtling, and A. Pucci, ACS Nano **8**, 4908 (2014).
35. H. Haus, *Waves and Fields in Optoelectronics* (Prentice-Hall, 1984).
36. S. Zhang, Z. Ye, Y. Wang, Y. Park, G. Bartal, M. Mrejen, X. Yin, and X. Zhang, Phys. Rev. Lett. **109**, 193902 (2012).
37. M.-A. Miri and A. Alù, Science **363**, eaar7709 (2019).